PHYSICAL REVIEW B **92**, 024416 (2015)

Reversible temperature-driven domain transition in bistable Fe magnetic nanostrips grown on Ru(0001)

A. Quesada,[1,*] M. Monti,[2] I. P. Krug,[3,4] N. Rougemaille,[5,6] F. Nickel,[3] D. M. Gottlob,[3] H. Doganay,[3] A. T. N'Diaye,[7] G. Chen,[8] A. Serrano,[1] K. F. McCarty,[9] J. F. Fernández,[1] C. M. Schneider,[3] A. K. Schmid,[8] and J. de la Figuera[2]

[1]*Instituto de Cerámica y Vidrio, CSIC, 28049 Madrid, Spain*
[2]*Instituto de Química Física "Rocasolano," CSIC, 28006 Madrid, Spain*
[3]*Research Center Jülich GmbH, Peter Grünberg Institute PGI 6, JARA FIT, D-52425 Jülich, Germany*
[4]*Institute for Optics und Atomic Physics, Technical University Berlin, D-10632 Berlin, Germany*
[5]*CNRS, Institut NÉEL, F-38042 Grenoble, France*
[6]*Université Grenoble Alpes, Institut NÉEL, F-38042 Grenoble, France*
[7]*Lawrence Berkeley National Laboratory, Advanced Light Source, Berkeley, California 94720, USA*
[8]*Molecular Foundry, Lawrence Berkeley National Laboratory, Berkeley, California 94720, USA*
[9]*Sandia National Laboratories, Livermore, California 94550, USA*

(Received 27 April 2015; revised manuscript received 29 June 2015; published 15 July 2015)

High-aspect-ratio Fe nanostrips are studied with real-space micromagnetic imaging methods. We experimentally demonstrate reversible switching from essentially homogeneous single-domain states at room temperature to multidomain diamond states at elevated temperature. This temperature-dependent magnetic bistability can be understood and modeled by accounting for the temperature dependence of the magnetocrystalline, shape, and magnetoelastic anisotropies. These results show how the transition temperature between two magnetic domain states can be tailored by controlling epitaxial strain and particle geometry, which may generate new opportunities for magnetic memory and logic device design.

DOI: 10.1103/PhysRevB.92.024416 PACS number(s): 75.75.Fk, 75.80.+q

I. INTRODUCTION

Mesoscopic magnetic elements feature a particularly rich diversity of interesting magnetic phenomena. Besides their fundamental relevance, these phenomena provide the opportunity to tailor and control magnetism through a variety of strategies [1–5]. One widely discussed aspect has been the observation of a single-domain threshold size in small magnetic particles [6]: below some critical size the magnetic ground state of individual elements can be a single-domain state, while multidomain flux-closure patterns are often more stable in larger structures [6,7]. Many basic studies have focused on the occurrence of magnetic domain patterns as a function of particle geometry [7–11]. Temperature-controlled single- to multidomain structure transitions remain less well explored; prior work on temperature-dependent magnetic phenomena in small elements includes thermally induced fluctuations such as magnetic bistability of Co nanodots switching from single-domain to vortex states [12] and superparamagnetic properties of small elements more generally [13].

Interest in thermally activated magnetic transitions is driven by applications in memory and logic devices [3,5], where some technologies depend on suppression of thermal effects (nonvolatility of memory, etc.), while other technologies depend on deliberate control of thermally activated effects (heat-assisted writing, etc.) [14]. In addition, the possibility of magnetic bistability is useful for applications in all-magnetic logic systems [15,16]. Thus, the ability to accurately predict and control thermally activated magnetic properties of small particles is important for a wide range of topics and calls for a validation of micromagnetic theory in comparative experimental/theoretical investigations.

Here we describe a model system to investigate temperature-driven, reversible magnetic transitions in individual high-aspect-ratio Fe magnetic particles epitaxially grown on a Ru(0001) substrate.

II. EXPERIMENT

Between 10 and 20 atomic layers (AL) of Fe were deposited by molecular beam epitaxy onto clean Ru(0001) substrates in 1×10^{-6} mbar O_2. The iron dose rate was 2 AL per minute and the substrate was kept at 880 K. The Ru substrates were cleaned by flash annealing at 1700 K under 5×10^{-8} mbar O_2. After growth, the films were cooled down to room temperature under ultrahigh vacuum (no O_2 atmosphere). The growth of the films was followed in real time by low-energy electron microscopy (LEEM) [17], in three different instruments. The first is an aberration-corrected combined LEEM/photoemission microscope (PEEM) at the UE56-1/SGM beamline at the BESSY synchrotron in Berlin [18]. The instrument allows acquiring x-ray circular magnetic dichroism (XMCD) images to either map the in-plane magnetization component for a given atomic element along the x-ray direction within the film with nanometer resolution, or to acquire selected area XMCD spectra as a function of photon energy. For XMCD images, two images at the Fe L_3 edge are taken with opposite photon helicity, and subtracted pixel by pixel. The second instrument is the spin-polarized low-energy electron microscope at Berkeley National Laboratory [19]. It is equipped with a spin-polarized electron source coupled to a spin manipulator that allows rotating the spin direction to any desired orientation relative to the sample [20]: this offers the ability to map the magnetization

*Author to whom all correspondence should be addressed: a.quesada@icv.csic.es

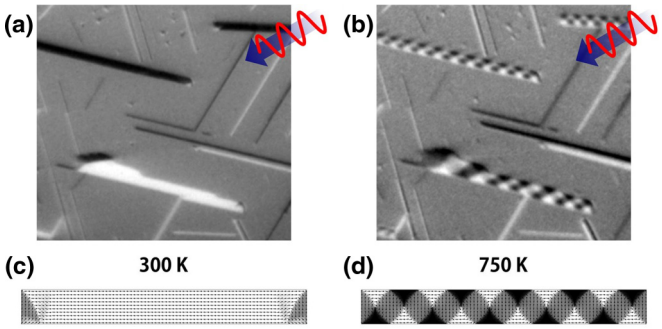

FIG. 1. (Color online) (a), (b) XMCD-PEEM gray scale images (11 μm field of view) at the L_3 x-ray absorption edge, where pixel brightness is proportional to the magnitude of the component of the magnetization vector along the incident photon beam direction. Imaging the same area at (a) 300 K and (b) 750 K shows temperature-dependent transition of several nanostrips from essentially single-domain C states to diamond multidomain states. OOMMF micromagnetic simulations show corresponding local spin directions of the single-domain C state (c) and the diamond multidomain state (d) (photon direction indicated by arrow/symbol in upper right corners).

in any desired direction, performing full three-dimensional magnetometry [21]. Using low-energy electron microscopy in microdiffraction mode (LEED), a 0.5-μm-diameter electron beam was diffracted on the nanostrips during LEED experiments performed at the third LEEM, an Elmitec instrument at Sandia National Laboratory. The energy of the incident electron beam was varied in the range of 15–50 eV.

III. RESULTS AND DISCUSSION

A. Magnetic transition

X-ray photoemission electron microscopy in magnetic circular dichroism mode (XMCD-PEEM) provides images of the micromagnetic structure of self-assembled high-aspect rectangular islands, or nanostrips, and reveals a striking temperature dependence. An image of an ensemble of nanostrips at room temperature is shown in Fig. 1(a), where well-defined homogeneous gray levels of the nanostrips indicate that they are in magnetic single-domain states; the in-plane micromagnetic structure of this so-called C state—note the slight contrast difference at the edge of the strips in Fig. 1(a), typical of the C state—is shown in a simulation result, Fig. 1(c). Taken by itself, this result is not surprising: when shape anisotropy dominates over other magnetic anisotropies, many types of high-aspect-ratio magnetic particles tend to be magnetized along their long axis in this type of state [9,22]. After elevating the sample temperature to 750 K, a second XMCD-PEEM image of the same elements is reproduced in Fig. 1(b), showing that some of the nanostrips have transformed into multidomain in-plane states; simulation results reproduced in Fig. 1(d) show the micromagnetic structure in more detail. By itself, this result is also expected: this type of flux-closure diamond multidomain state can be seen in many other types of magnetic structures [7,8,11,23,24].

The interesting aspect of this system is that, unlike the cited previous studies [7–9,11,12,24], we find that the transitions between these two states are reliably reversible under temperature cycling, and that the critical transition temperatures of individual nanostrips depend on their width. Indeed, we see that narrow nanostrips remain in a single-domain state up to their Curie temperature (T_c). In the remainder of this paper we address the physical origins of this remarkable dependence of magnetic domain states on temperature.

B. Structure and composition

We start by summarizing the growth and composition of the nanostrips. Following the formation of an atomically thin FeO [25] wetting layer, deposition of Fe on Ru(0001) at a rate of two atomic monolayers per minute in 10^{-6} Torr oxygen at 880 K substrate temperature produces the nanostrips discussed here. The FeO wetting layer shows no magnetic contrast in XMCD-PEEM images (see Fig. 1), which is plausible because bulk FeO is antiferromagnetic with a Néel temperature below room temperature [26]. To determine the composition of the nanostrips, we used spectroscopic imaging by scanning the photon energy while collecting XMCD-PEEM images. This facilitates extraction of XMCD spectra from individual features and a spectrum collected from a single nanostrip is reproduced in Fig. 2(a). It matches those reported for Fe and clearly lacks the distinct peak splitting reported for magnetic iron- oxides [see Fig. 2(b)] [27,28], thus showing that the nanostrips are composed of metallic Fe. (Due to the preparation in the presence of oxygen, we assume the Fe nanostrips are covered with an atomically thin FeO layer, but the ultrathin oxide surface layer does not significantly affect the XMCD spectra.)

Next we address the crystalline and geometric structure of the nanostrips. Fe grown on Ru(0001) surfaces under ultrahigh-vacuum conditions is known to form bcc(110) islands in Kurdjumov-Sachs epitaxial orientation [29], where the bcc $[1\bar{1}1]$ axis is parallel to the hcp $[11\bar{2}0]$ direction. In this epitaxial relationship, two bcc coincidences are possible for each close-packed direction of the underlying hcp lattice, oriented at $+/-5^\circ$ of the three equivalent $[11\bar{2}0]$ directions [30]. LEED), shown in Fig. 2(d), reveals two diffraction patterns, rotated by 5° with respect to each other. As the 0.5-μm-diameter electron beam illuminates both a section of a nanostrip and a section of the adjacent substrate region, the angular alignment of these patterns is consistent with the expected $+/-5^\circ$ coincidence of the Kurdjumov-Sachs epitaxy of Fe/Ru(0001) [31]. This result indicates that even if a FeO wetting layer covers most of the Ru(0001) surface, the Fe nanostrips grow on top of the bare Ru.

The diffraction experiments also reveal a family of diffraction spots that move across the screen as a function of beam energy. To highlight the moving diffraction spots, the pattern reproduced in Fig. 2(d) was generated by image integrating over the energy range from 15 to 50 eV. As a result, the spot motion appears as streaks. The moving spots arise from edge facets that are inclined with respect to the surface plane, indicating a trapezoidal cross section of the nanostrips. The energy-dependent displacements of the facet spots are along $[1\bar{1}0]$ and $\bar{1}10$ directions, which implies that the edge facets are tilted away from the (110) surface normal towards these directions; consequently the long axis of the nanostrips must be oriented along the [001] direction. This

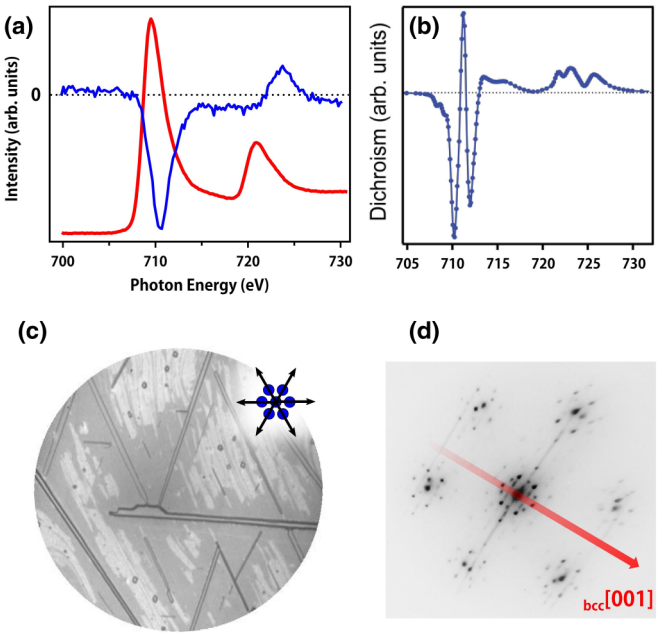

FIG. 2. (Color online) (a) Microspectroscopy from an individual nanostrip (x-ray absorption shown in red). Dichroic spectra (in blue) from a nanostrip show that the Fe L_3 edge has a shape corresponding to elemental Fe, rather than to an iron oxide. (b) shows dichroic spectra at the Fe L_3 edge corresponding to Fe_3O_4 (reproduced from Ref. [26], with permission). (c) LEEM image (20 μm field of view) showing the formation of nanowires on Ru(0001) and highlighting the $60^\circ + / - 5^\circ$ angles between relative orientations of strips and the $+/-5^\circ$ angles between the strips and the underlying compact directions of the sketched hexagonal Ru(0001). (d) Microdiffraction from an individual nanostrip. The sum of a series of LEED patterns collected at different energies (from 15 to 50 eV) shows fixed diffraction spots from flat parts of the surface as well as streaks due to a family of diffraction spots that move as a function of energy. The moving diffraction spots originate from edge facets. The red arrow indicates the long axis direction of the nanostrip, perpendicular to the lines of motion of the streaked LEED spots.

picture implies six growth directions of nanostrips, oriented at $+/-5^\circ$ of the three close-packed directions of the substrate. Indeed the resulting 10° angle between individual nanostrips is often seen in our images. For instance, Fig. 2(c) presents a LEEM image where Fe strips with varying thicknesses are portrayed. Thinner strips appear as straight black lines, while wider ones are seen as transparent elongated rectangles at the particular electron energy employed. Smaller dots and islands correspond to FeO_x [25]. The outlines of a large number of individual strips were measured, showing that widths a and lengths c are in the ranges $a = 80$–1400 nm and $c = 1.5 - 15\,\mu$m and the smallest aspect ratio observed is of the order of $n = 7$. Taking into account the area fraction covered by nanostrips and the total dose of deposited Fe, we conclude that their average thickness is around 25 nm, and it is plausible to expect a significant dispersion of thickness values.

C. Discussion and micromagnetic model

Now we focus on the origin of the observed magnetic transition. A clue for the understanding is provided by the correlation between the width and transition temperature of the nanostrips; the widest strips transition to multidomain states at the lowest critical temperature, while in the narrowest strips single-domain states persist up to the Curie point. To quantify these observations, ensembles of nanostrips were heated to selected values of temperature and their width-dependent magnetic states were measured by spin-polarized LEEM.

For each temperature (T), Fig. 3(a) plots widths of the strips, using blue dots for those found to be in single-domain C states and red dots for those found in multidomain diamond states. The plot clearly shows a diagonal phase boundary separating the two states. In addition, the difference between data collected while heating or cooling reveals a hysteresis in the transition of about 350 °C. We assume this hysteresis to be the consequence of the existence of energy barriers between the two states that need to be overcome [12]. Thermal fluctuations aid overcoming these barriers and play a role in the dynamics associated with this magnetic transition. However, in order to understand and model its origin, the balance between the relevant magnetic anisotropies must be considered.

When the effective anisotropy is aligned with the long axis of the nanostrips, single-domain states are the expected ground state. For diamond multidomain patterns to be stable, an anisotropy perpendicular to the long axis of the nanostrips must be present. Given that ⟨001⟩ directions are the easy axes of bcc Fe [32], both magnetocrystalline and shape anisotropy vectors are parallel to the nanostrips and favor single-domain states. This suggests that additional sources of anisotropy must be taken into account. Surfaces and interfaces of the nanostrips might affect anisotropy in the out-of-plane direction, but recalling that the $t = 25$ nm average thickness of the nanostrips is more than an order of magnitude smaller that their width, it is not likely that surface anisotropy on the edge facets is sufficient to stabilize in-plane perpendicular anisotropy.

Two sources of magnetoelastic anisotropy should be considered: (1) the substrate-induced lattice mismatch and (2) the thermal strain consequence of the different thermal expansion coefficients of Fe and Ru. Taking into account that thermal strain is proportional to $\Delta T = T_{\text{observation}} - T_{\text{growth}}$, where $T_{\text{observation}}$ is the T at which the XMCD-PEEM image is obtained and $T_{\text{growth}} = 880$ K, the T at which the sample was grown [24], the second source of magnetoelastic anisotropy vanishes upon annealing and approaching growth temperature.

On the other hand, biaxial strain (perpendicular and parallel to the strips) induced by the lattice mismatch will be considered. Along $\langle 1\bar{1}0\rangle$, strain is tensile [33] and the associated magnetostriction constant λ_{110} Fe, being a linear combination of λ_{100} and λ_{111} [34], is negative below 470 K and positive above [35]. This implies that the magnetoelastic anisotropy originated by strain along $\langle 1\bar{1}0\rangle$ changes its direction at 470 K from parallel (at low temperature) to perpendicular (at high temperature) to the strips. The magnetostriction constant of Fe along ⟨001⟩ λ_{100} is positive and increases monotonously between room temperature and 750 K, from 20×10^{-6} to 30×10^{-6} [35]. The compressive strain of Fe/Ru along ⟨001⟩ [33] and the positive value of λ_{100} imply a magnetoelastic easy axis perpendicular to the long axis of the nanostrips at all temperatures studied. The transition can thus be qualitatively explained: magnetocrystalline anisotropy, which is aligned with the long axis, decreases as a function

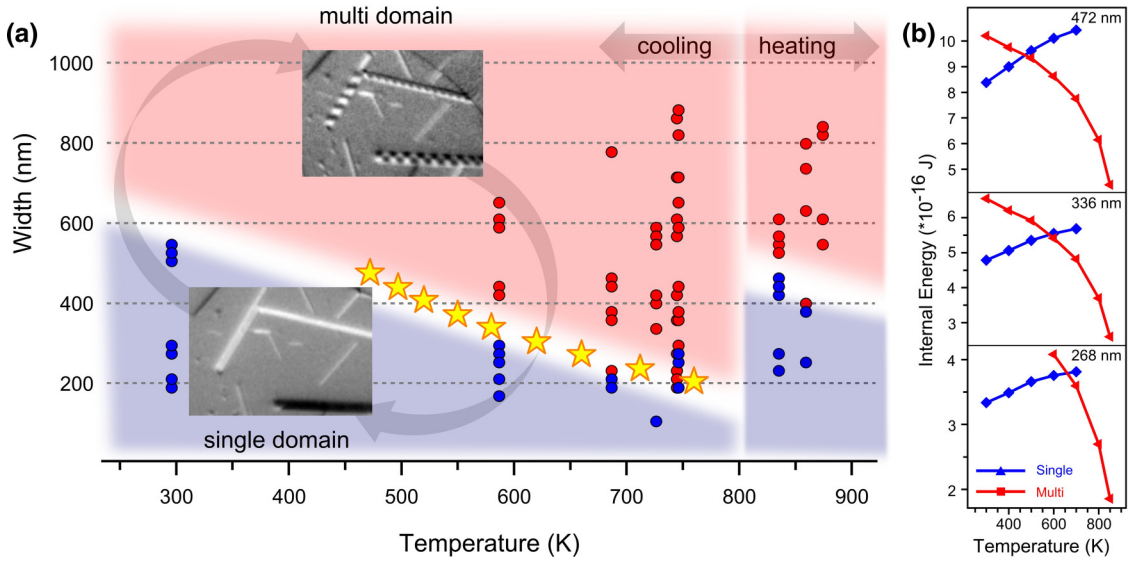

FIG. 3. (Color online) (a) Plot summarizing domain state measurements on nanostrips as a function of temperature and width. Red/blue triangle symbols indicate experimentally observed multidomain/single-domain configurations, respectively. Yellow star symbols indicate the transition critical width calculated from micromagnetic simulations, in good agreement with the experimental data. Two XMCD-PEEM images ($6\,\mu\text{m} \times 4\,\mu\text{m}$ field of view) are inserted to highlight each state. (b) Internal energy as a function of temperature calculated by micromagnetic simulations corresponding to single- and multidomain configurations for nanostrips with three different widths (472, 336, and 268 nm) and constant aspect ratio of 8.

of increasing temperature [32]. In contrast, the magnetoelastic anisotropy (K_{me}) perpendicular to the wires, caused by lattice mismatch, increases with temperature favoring magnetization aligned perpendicular to the long axis. It should be noted that shape anisotropy decreases with temperature [32].

To validate this idea we constructed a quantitative micromagnetic model employing the object oriented micromagnetic framework (OOMMF) code [36]. We start by estimating the temperature-dependent strain state of the nanostrips. Given the thickness range of the Fe strips, these must be mostly relaxed [37]. However, small residual strains cannot be neglected here: a residual strain in the range $\varepsilon = 0.1\%$–0.5%, which has been reported in Fe films for comparable thicknesses and lattice mismatch [38], can stabilize a relatively large magnetoelastic anisotropy K_{me}. Taking into account that at elevated temperatures λ_{110} is roughly between six and four times smaller than λ_{100}, we will consider for simplicity only magnetoelastic anisotropy originated along $\langle 001 \rangle$. From the relation [24]

$$K_{me} = \frac{3}{2}\frac{E\lambda_{100}\varepsilon}{1-\nu}, \tag{1}$$

where $E = 211\,\text{GPa}$ is the Young modulus, $\upsilon = 0.29$ is the Poisson ratio of Fe, and substituting the value of λ_{100} at 750 K, $K_{me} = 4 \times 10^4\,\text{J m}^{-3}$ is obtained for $\varepsilon = 0.3\%$.

Nanostrips with a fixed aspect ratio of $n = 8$ and different widths, lengths, and thicknesses were modeled in the OOMMF simulations. A cubic anisotropy is used to describe bulk Fe. Two main directions are defined, the third one being their vector product. These two directions are $\langle 100 \rangle$ and $\langle 0\bar{1}1 \rangle$. The magnetoelastic anisotropy K_{me} is approximated as uniaxial and perpendicular to the $\langle 001 \rangle$ long axes of the nanostrips, and its value is estimated employing the equation reported above. The magnitude of K_{me} was calculated based on the temperature dependence of λ_{100}. The temperature dependence of magnetocrystalline anisotropy, exchange stiffness (A), and saturation magnetization (M_s) were taken into account, assuming bulk Fe literature values [32,35]. The following room temperature values were employed: $A = 21 \times 10^{-12}\,\text{J m}^{-1}$, $M_s = 1713\,\text{kA m}^{-1}$, $K_1 = 4.8 \times 10^4\,\text{J m}^{-3}$, and $K_{me} = 2 \times 10^4\,\text{J m}^{-3}$. The cell size in all simulations reported here is $4 \times 4 \times 20\,\text{nm}^3$ and the damping parameter is set to 1.

Moreover, and given the lack of a direct strain measurement, a broad range of K_{me} values were considered in additional simulations. Below $1 \times 10^4\,\text{J m}^{-3}$, K_{me} is not strong enough to stabilize the multidomain structure at any temperature below the Curie point. Between 1 and $4 \times 10^4\,\text{J m}^{-3}$, both the single and multidomain structures are stable and the transition is reproduced. Above $4 \times 10^4\,\text{J m}^{-3}$, the strips remain in a multidomain state at all temperatures between RT and T_c.

Figure 3(b) shows the results of OOMMF simulations where we computed the internal energy of the C-state and diamond configurations, corresponding to different temperatures, for nanostrips with three different widths and constant aspect ratio $n = 8$. The simulations do not take explicitly into account thermal effects, except for the fact that they are implicit in the magnetic parameters utilized. Upon increasing temperature, the energy associated with the C state increases, until crossover points with the energy of the diamond state are observed. The crossing points correspond to the critical points at which the transition occurs. Simulating the evolution of internal energies for nanostrips with different widths, the resulting transition points are shown as yellow star symbols in Fig. 3(a). Agreement with the experimental results shows

that this model, accounting for temperature dependence of shape anisotropy, magnetocrystalline anisotropy, and magnetoelastic anisotropy predicts the size dependence of critical temperatures at which the nanostrips undergo the domain-state transition.

IV. CONCLUSIONS

In summary, studying self-assembled high-aspect-ratio nanostrips we observe reversible transitions between two stable domain configurations. Fe nanostrips switch between a single-domain state at room temperature and a flux-closure multidomain diamond configuration above size-dependent critical temperatures. A micromagnetic model capturing magnetocrystalline, shape, and magnetoelastic anisotropies predicts the temperature and size dependence of the magnetic domain states. Our findings show that controlling the strain state and geometry of small magnetic elements enables tailoring the temperature at which a transition between two magnetic states with very different properties occurs.

ACKNOWLEDGMENTS

The authors acknowledge financial support from the Spanish MINECO through Projects No. MAT2012-38045-C04-01 and No. MAT2013-48009-C4-1-P and from the European Commission through the project NANOPYME FP7-NMP-2012-SMALL-6 NANOPYME (No. 310516). Experiments performed at the Molecular Foundry, National Center for Electron Microscopy, Lawrence Berkeley National Laboratory, were supported by the Office of Science, Office of Basic Energy Sciences, Scientific User Facilities Division, of the U.S. Department of Energy under Contract No. DE-AC02-05CH11231. A.Q. and M.M. would like to acknowledge financial support from the Spanish Ministerio de Economía y Competitividad through the Juan de la Cierva program, and through a FPI contract.

A.Q. and M.M. contributed equally to the manuscript.

[1] R. O. Cherifi, V. Ivanovskaya, L. C. Phillips, A. Zobelli, I. C. Infante, E. Jacquet, V. Garcia, S. Fusil, P. R. Briddon, N. Guiblin, A. Mougin, A. A. Ünal, F. Kronast, S. Valencia, B. Dkhil, A. Barthélémy, and M. Bibes, Nat. Mater. **13**, 345 (2014).

[2] S. Mangin, M. Gottwald, C.-H. Lambert, D. Steil, V. Uhlíř, L. Pang, M. Hehn, S. Alebrand, M. Cinchetti, G. Malinowski, Y. Fainman, M. Aeschlimann, and E. E. Fullerton, Nat. Mater. **13**, 286 (2014).

[3] R. L. Stamps, S. Breitkreutz, J. Åkerman, A. V. Chumak, Y. Otani, G. E. W. Bauer, J.-U. Thiele, M. Bowen, S. A. Majetich, M. Kläui, I. L. Prejbeanu, B. Dieny, N. M.Dempsey, and B. Hillebrands, J. Phys. D **47**, 333001 (2014).

[4] C. F. Vaz, J. C. Bland, and G. Lauhoff, Rep. Prog. Phys. **71**, 056501 (2008).

[5] X. Marti, I. Fina, C. Frontera, J. Liu, P. Wadley, Q. He, R. J. Paull, J. D. Clarkson, J. Kudrnovský, I. Turek, J. Kuneš, D. Yi, J.-H. Chu, C. T. Nelson, L. You, E. Arenholz, S. Salahuddin, J. Fontcuberta, T. Jungwirth, and R. Ramesh, Nat. Mater. **13**, 367 (2014).

[6] W. F. Brown, Ann. N. Y. Acad. Sci. **147**, 463 (1969).

[7] R. Hertel, O. Fruchart, S. Cherifi, and P.-O. Jubert, S. Heun, A. Locatelli, and J. Kirschner, Phys. Rev. B **72**, 214409 (2005).

[8] R. Zdyb, A. Pavlovska, M. Jałochowski, and E. Bauer, Surf. Sci. **600**, 1586 (2006).

[9] N. Rougemaille and A. K. Schmid, J. Appl. Phys. **99**, 08S502 (2006).

[10] R. Hertel, Z. Metallkd. **93**, 957 (2002).

[11] S. Cherifi, R. Hertel, J. Kirschner, H. Wang, R. Belkhou, A. Locatelli, S. Heun, A. Pavlovska, and E. Bauer, J. Appl. Phys. **98**, 043901 (2005).

[12] H. F. Ding, A. K. Schmid, D. Li, K. Y. Guslienko, and S. D. Bader, Phys. Rev. Lett. **94**, 157202 (2005).

[13] V. Skumryev, S. Stoyanov, Y. Zhang, G. Hadjipanayis, D. Givord, and J. Nogues, Nature (London) **423**, 850 (2003).

[14] M. H. Kryder, E. C. Gage, T. W. McDaniel, W. A. Challener, R. E. Rottmayer, G. Ju, Y.-T. Hsia, and M. F. Erden, Proc. IEEE **96**, 1810 (2008).

[15] J.-G. Zhu, Y. Zheng, and G. A. Prinz, J. Appl. Phys. **87**, 6668 (2000).

[16] A. Chiolerio, P. Allia, and M. Graziano, J. Magn. Magn. Mater. **324**, 3006 (2012).

[17] J. Figuera and K. McCarty, in *Surface Science Techniques*, edited by G. Bracco and B. Holst (Springer, Berlin, 2013), Vol. 18, pp. 531–561.

[18] C. M. Schneider and G. Schönhense, Rep. Prog. Phys. **65**, 1785 (2002).

[19] N. Rougemaille and A. K. Schmid, Eur. Phys. J. Appl. Phys. **50**, 20101 (2010).

[20] T. Duden and E. Bauer, Rev. Sci. Instrum. **66**, 2861 (1995).

[21] F. El Gabaly, S. Gallego, C. Muñoz, L. Szunyogh, P. Weinberger, C. Klein, A. K. Schmid, K. F. McCarty, and J. de la Figuera, Phys. Rev. Lett. **96**, 147202 (2006).

[22] Z. Liu, P.-C. Chang, C.-C. Chang, E. Galaktionov, G. Bergmann, and J. G. Lu, Adv. Funct. Mater. **18**, 1573 (2008).

[23] W. Brückner, J. Thomas, R. Hertel, R. Schäfer, and C.M. Schneider, J. Magn. Magn. Mater. **283**, 82 (2004).

[24] J.-Y. Chauleau, B. J. McMorran, R. Belkhou, N. Bergeard, T. O. Menteş, M. Á. Niño, A. Locatelli, J. Unguris, S. Rohart, J. Miltat, and A. Thiaville, Phys. Rev. B **84**, 094416 (2011).

[25] M. Monti, B. Santos, A. Mascaraque, O. Rodríguez de la Fuente, M. A. Niño, T. O. Menteş, A. Locatelli, K. F. McCarty, J. F. Marco, and J. de la Figuera, Phys. Rev. B **85**, 020404 (2012).

[26] R. M. Cornell and U. Schwertmann, *The Iron Oxides* (Wiley-VCH, Weinheim, 2003).

[27] E. Pellegrin, M. Hagelstein, S. Doyle, H. O. Moser, J. Fuchs, D. Vollath, S. Schuppler, M. A. James, S. S. Saxena, L. Niesen, O. Rogojanu, G. A. Sawatzky, C. Ferrero, M. Borowski, O. Tjernberg, and N. B. Brookes, Phys. Status Solidi **215**, 797 (1999).

[28] B. Santos, E. Loginova, A. Mascaraque, A. K. Schmid, K. F. McCarty, and J. de la Figuera, J. Phys.: Condens. Matter **21**, 314011 (2009).

[29] J. Kołaczkiewicz and E. Bauer, Surf. Sci. **423**, 292 (1999).

[30] S. Andrieu, M. Piecuch, and J. F. Bobo, Phys. Rev. B **46**, 4909 (1992).
[31] T. Allmers and M. Donath, New J. Phys. **11**, 103049 (2009).
[32] B. D. Cullity and C. D. Graham, *Introduction to Magnetic Materials* (Wiley, New York, 2008), pp. 115–149.
[33] D. Tian, H. Li, F. Jona, and P. M. Marcus, Solid State Commun. **80**, 783 (1991).
[34] B. D. Cullity and C. D. Graham, *Introduction to Magnetic Materials* (Wiley, New York, 2008), pp. 241–273.
[35] E. W. Lee, Rep. Prog. Phys. **18**, 184 (2002).
[36] M. J. Donahue and D. G. Porter, Interagency Report NISTIR 6376, National Institute of Standards and Technology, Gaithersburg, MD, 1999 (unpublished).
[37] D. Sander, A. Enders, C. Schmidthals, D. Reuter, and J. Kirschner, J. Magn. Magn. Mater. **177-181**, 1299 (1998).
[38] D. Sander, A. Enders, and J. Kirschner, J. Magn. Magn. Mater. **199**, 519 (1999).